Mechanism of silica nanoparticles removal in an isopropyl alcohol/water solution with an anion exchange membrane

Fujimura, Yu
Kawakatsu, Takahiro
Nakagawa, Keizo
Shintani, Takuji
Yoshioka, Tomohisa

(Citation)
Journal of Molecular Liquids,347:118366

(Issue Date)
2022-02-01

(Resource Type)
journal article

(Version)
Accepted Manuscript

(URL)
https://hdl.handle.net/20.500.14094/90009120

Mechanism of silica nanoparticles removal in an isopropyl alcohol/water solution with an anion exchange membrane

Yu Fujimura,[1,2,*] Takahiro Kawakatsu,[1] Keizo Nakagawa,[2,3] Takuji Shintani,[2,3] and Tomohisa Yoshioka[2,3]

[1]Research and Development Division, Kurita Water Industries Ltd., 1-1 Kawada, Nogi-machi, Simotsuga-gun, Tochigi 329-0105, Japan

[2]Graduate School of Science, Technology, and Innovation, Kobe University, 1-1 Rokkodai, Nada, Kobe 657-8501, Japan

[3]Research Center for Membrane and Film Technology, Kobe University, 1-1 Rokkodai, Nada, Kobe 657-8501, Japan

Keywords: Silica nano particle; Anion exchange membrane; Isopropyl alcohol; Molecular dynamics; Density functional theory; Surface cleaning

*Corresponding: y.fujimura95@kurita-water.com

Abstract

Isopropyl alcohol (IPA) is frequently used for cleaning fine patterns of semiconductor devices and technology to remove the fine particles from IPA is desired in the industry. In this study, an anion exchange membrane was used to remove silica nanoparticles, and zeta potential measurements were conducted on the particles and the membrane in an IPA/water solution. Also, molecular dynamics (MD) and density functional theory (DFT) simulations were conducted to clarify the removal mechanism. As the portion of IPA increased in the ratio of the IPA/water solution, the zeta potential of the particles remained negative, while that of the anion exchange membrane in the solvent turned from positive to negative and the particles were not removed. The reason for this behavior was examined by studying the movement of chloride ions near the membrane using MD simulations and by constructing an energy-level

diagram using DFT theory simulations. As a result, we found that when the IPA ratio was increased, the chloride ions and solvent molecules in the vicinity of the anion exchange membrane donated electrons. This development could be useful when searching for more effective materials for the removal of fine contaminative particles.

1. Introduction

In recent years, the development of AI and other technologies has led to further performance improvements in semiconductors. One of the main trends has been miniaturization that improves integration density and reduces power consumption for a technology node that is approaching 3 nm. Semiconductor devices are made by repeatedly stacking and etching materials. In between these processes, there is always a wet cleaning process using liquid, and ultrapure water has played a role until now. However, as semiconductors become increasingly miniaturized, pattern collapse due to the surface tension of ultrapure water is becoming a problem. Against this backdrop, the low surface tension of IPA makes it suitable for cleaning microfabricated structures, thus cleaning with IPA is indispensable for currently semiconductor cleaning process. Furthermore, it is increasingly being used in conjunction with ultrapure water to clean the wafers used in semiconductor manufacturing processes [1-12]. As semiconductor structures have become smaller, however, the restrictions for the amount of impurities in ultrapure water, especially particulates, has become stricter every year. The 2020 revision of the International Roadmap for Devices and Systems (IRDS) for particulates in IPA indicates that the number of particulates in 1L should be reduced to 50 or less [13]. Semiconductor structures are expected to become even smaller and/or more complex in the future, and the use of IPA for cleaning them is also expected to increase in the future. Although electronic-grade (EL grade) IPA is available from various suppliers for use by the electronics industry, it would be desirable for the purity of IPA to be much improved and for the environmental impact to be reduced via a mechanism such as on-site filtration with a filter similar to those used in the production of ultrapure water. Filters for solvents are investigated and improved daily [14–22], but they are used mainly for size exclusion to remove fine particles.

Methods of particle removal using charge and polarity have been reported only in aqueous systems [23–26], and more detailed removal mechanisms have not been introduced. IPA is often mixed with water in the cleaning process [1,2], and the behavior of the solid interface when using a mixture of water and alcohol has been investigated [27–30]. Although there have been extensive investigations on particle removal in ultrapure water [31–34], the effect that the interaction between the particles and the membrane structure can exert on the particle removal mechanism in the solvent has yet to be clarified. Furthermore, the chemical states of the membrane and particle surfaces are expected to change with respect to charge and coordination due to the influence of the solvent species. Computer simulations have been used to evaluate the effect that water molecules and IPA molecules exert on polymer surfaces [35,36], but few studies have focused on the interaction between a membrane and particle surfaces that undergo surface-state changes.

In this study, we investigated the particle removal mechanism in organic solvents zeta potential measurements of an ion exchange membrane and the particle surfaces in an IPA/water solution during particle removal tests. The effects that solution molecules and ions exert on the membrane were evaluated using MD and DFT simulations. The solvent was a mixture of IPA and water in various ratios, and silica nanoparticles (SNP) served as the model particles.

2. Experimental and simulation models

2.1. SNP removal and zeta potential measurement

2.1.1 SNP removal in an IPA/water solution

SNP adsorption and removal tests were carried out using an anion exchange membrane. The anion exchange membrane used was a Neocepta AHA (ASTOM Corporation), which was immersed for more than 1 day in solutions containing various levels of IPA in the ratio. The model particles used were 30 nm SNPs (sicastar®, Micromod Partikeltechnologie GmbH, polydispersity indices < 0.2). A 100 cm^2 anion exchange membrane was immersed in a solution containing 10 ppm of SNPs and was stirred for 30 min over an additional 1-3 days. Afterwards, the total silica concentration was analyzed by heated dissolution-molybdenum

blue absorption spectrophotometry with sodium carbonate. The adsorption removal ratio in each solution was calculated using Equation 1.

$$Removal\ ratio\ [\%] = \frac{(C_{SNP}\ before\ test) - (C_{SNP}\ after\ test)}{(C_{SNP}\ before\ test)} \times 100 \quad \text{(Equation 1)}$$

In the case of 0% IPA in the ratio, the test was also conducted by the additions of 10 and 100 ppm of sodium chloride after stirring for 1 day to investigate the effect of Cl^- ions.

2.1.2. Zeta potential measurement of SNP and an anion exchange membrane in an IPA/water solution

The zeta potential of AHA in each IPA/water solution was measured using a Zetasizer Nano ZS (Malvern Panalytical). A flat-plate zeta potential measurement cell (ZEN1020) was used, and 50 nm SNPs (sicastar®, Micromod Partikeltechnologie GmbH, polydispersity indices < 0.2) served as the tracer particles. KCl was dissolved in water to a concentration of 10 mM. The membranes were immersed in each solution for 10 min after being fixed on the measurement stage and replace the water in the membrane with the solution. The physical properties in each solution are shown in Table 1.

Table 1 Physical properties of IPA/water solutions [37–39]

IPA ratio [vol%]	Density [g/cm^3]	Refractive index [-]	Viscosity [10^3Pa s]	Dielectric constant [-]
0	1.00	1.333	1.0	80
10	0.98	1.339	1.4	70
30	0.96	1.352	2.6	58
50	0.92	1.363	3.4	47
70	0.88	1.371	3.5	35
90	0.83	1.377	2.6	22
100	0.79	1.378	2.4	18

The zeta potential of the SNPs in each version of the IPA/water solutions was measured using a Zetasizer Nano ZS (Malvern Panalytical) with a solution of 250 ppm of 30 nm SNP model particles (sicastar®, Micromod Partikeltechnologie GmbH, polydispersity indices < 0.2).

2.2. Molecular dynamics simulation

This simulation used BIOVIA Materials Studio® 2020 software. In view of the simulation models, all atomic size is displayed in a unified manner. *Amorphous Cell* module was used to pack the unit cells of the membrane model with the solvent molecules, and *Forcite Plus* module was used to stabilize the simulation model and perform molecular dynamics simulations. COMPASS II [40,41] was used for a force field. COMPASS II is an improved and developed force field from COMPASS, whose potential parameters are shown in [40]. The potential parameters of COMPASS are given in [40]. Validation of COMPASS II for several materials is given in [41]. Additionally, in references [42–44], physical properties such as diffusion coefficients and densities of organic and inorganic materials are evaluated using COMPASS, and good results are reported in comparison with experimental values. Especially, the reference [44] evaluates the densities of water and IPA calculated using COMPASS, and reports that the error is only a few percent. Based on these references, we considered that the COMPASS force field would be applicable for simulations of water/IPA systems studied in this work. The potential functional forms of COMPASS II have been showed in Supplementary Materials.

2.2.1. Membrane model

In order to represent and simulate the structure of the AHA membrane, styrene and Divinylbenzene (DVB) monomers were used as crosslinking agents that formed a polymer. The polymer was constructed by connecting styrene and DVB at a ratio of 14:1 that achieved a crosslinking ratio of 7~8% [45,46]. The membrane model was prepared by packing 15 styrene-DVB polymer chains as described above and 210 Cl^- ion exchange group counterions into a unit cell at a density of 1.05 g/cc. The prepared styrene-DVB polymer model in chemical structural formula model and membrane slab model are shown in Fig. 1. The size of

the unit cell was set as $a = b = 60$ Å. The c-axis of the unit cell was automatically determined at $c = 21.177$ Å when the loading number, density, and the a- and b-axis lengths were determined. Also, three-dimensional periodic boundary conditions were adopted. After optimizing the structure of the membrane model using molecular mechanics, MD simulations were performed under NPT ensemble conditions (2.0 GPa, 298 K, 40 ps, Time step = 1.0 fs) with a constant number of molecules, pressure, and temperature. The cell size after MD simulation under NPT ensemble condition was a = b = 57.035 Å and c = 19.4086 Å. To represent the conditions of immersion into an IPA/water solution, solvent molecules of different concentrations were packed into the vacancies in the membrane model.

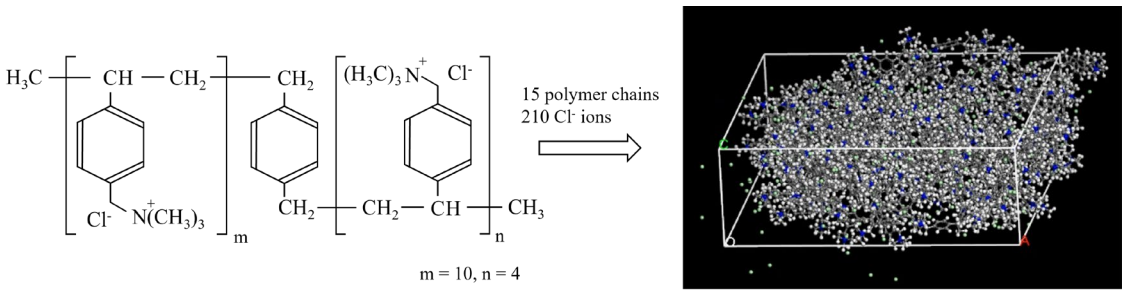

Fig. 1 Chemical structural formula of Styrene-DVB polymer model and membrane slab model including Cl^- ions (Atom colors: white, H; gray, C; blue, N; and, light green, Cl^-)

Table 2 Number of atoms of Styrene-DVB polymer model and membrane slab model

Atom	Styrene-DVB polymer model	Membrane slab model
C	178	2670
H	266	3990
N	14	210
Cl^-	14	210

Since the model used in the MD simulation was focused on a small region of the actual membrane, it was difficult to use the physical properties of an actual membrane. To avoid this problem, the density of the anion exchange resin was used as a reference. Membrane models with densities ranging from 1.05 to 1.2 g/cc were prepared and MD simulations were performed as described above to optimize the structure. As a result, 1.05 g/cc, which is the

lowest total level of energy, was adopted as the density of the membrane model. In the MD simulation under NPT ensemble conditions, Breandsen [47] was used as the pressure adjustment algorithm with a decay constant of 0.1 ps and a cutoff distance of 1.55 nm. The density of the membrane model after MD simulation was 1.22 g/cc. Although there was an error of approximately 15% with respect to the actual density, the priority in this simulation was to avoid pinholes in the membrane model.

2.2.2. Model for evaluating the differences in Cl^- ion diffusion in IPA/water solutions

In order to evaluate the differences in the diffusion of Cl^- ions in an IPA/water solution, models containing solvent molecules with the ratios of interest and Cl^- ions were prepared. MD simulations under NVT ensemble conditions were performed for 250 ps with a constant number of molecules and volume at a constant temperature of 298 K and the time step was set 1.0 fs. The Nose temperature adjustment algorithm was used in this simulation [48–50] In addition, layer models containing solvent molecules with the ratios of interest were connected along the c-axis of the membrane model to create a model that could be used to evaluate the diffusion of Cl^- ions. The a- and b-axis lengths of the layer model were aligned with those of the membrane model, and the c-axis length was set to 40 Å. The three-dimensional periodic boundary conditions were adopted. The connected slab model is shown in Fig. 2 and number of solution molecules in each simulation model is shown in Table 3. Note that when the membrane model and the layer model containing solvent molecules are combined, the maximum and minimum heights of the surface waviness of the membrane model are considered as the maximum and minimum values of the unit cell, and therefore the length of the combined model in the C-axis direction is somewhat larger than the sum of the thickness of the membrane model (19.41 Å) and the solution model (40 Å), which was 76.57 Å. After MD simulation under NVT ensemble conditions, the *c*-axis distribution profiles of the Cl^- ions were obtained and compared with the distribution profiles at t = 0, 100, and 250 ps.

Table 3 Number of solution molecules in each simulation models to evaluate the differences in Cl^- ion diffusion

IPA ratio*	Number of IPA molecules	Number of water molecules
100%	1109	0

90%	1088	513
70%	873	1588
50%	641	2719
30%	394	3899
10%	134	5120
0%	0	5747

* This ratio is vol% based on the volume of the pure component before mixing.

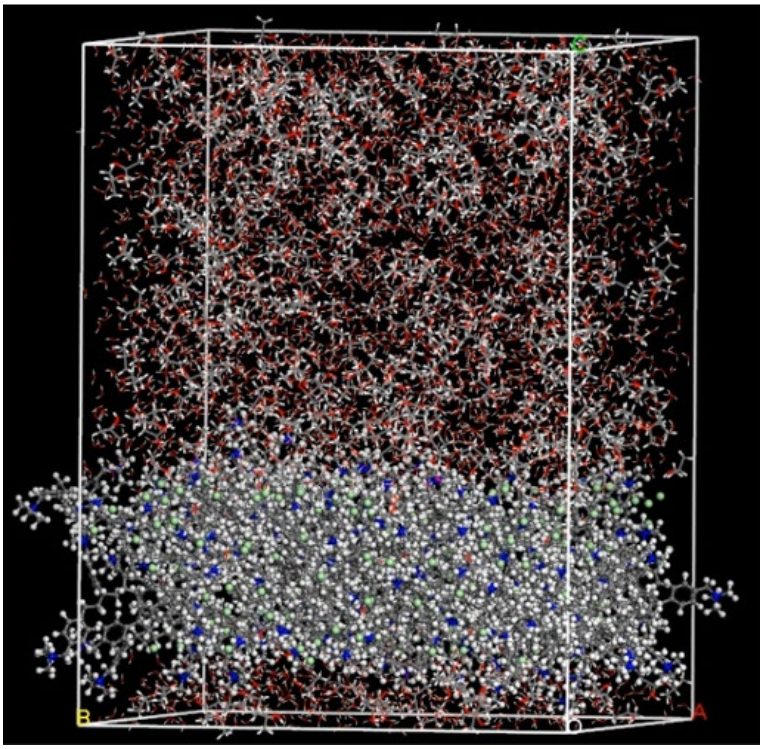

Fig. 2 Simulation model to evaluate the differences in Cl^- ion diffusion; IPA ratio = 30% model is shown as a sample (Atom colors: white, H; gray, C; red, O; blue, N; and, light green, Cl^-)

2.3. Density functional theory simulation for the membrane slab model

DFT simulation was used to simulate the HOMO/LUMO energy levels of the ion exchange membrane. This simulation used the BIOVIA Materials Studio® 2020 software, and the calculations were performed with *DMol*^{3} module, which can perform quantum mechanical simulations based on density functional theory.

The membrane model was prepared by packing one styrene-DVB polymer chain and 14 Cl^- ions, which are the counterions of the ion exchange groups, into a unit cell with a density of

1.05 g/cc. Also, three-dimensional periodic boundary conditions were adopted. The size of the unit cell after packing was $a = b = c = 16.985$ Å. The configuration of Cl^- ions was determined to be located within 5 Å from N atoms according to the simulated annealing method using Monte Carlo sampling with N as the target atom in the polymer [51,52]. The number of cycles and Monte Carlo steps per cycle was set to 5 and 50000 each other. The slab membrane model is shown in Fig. 3.

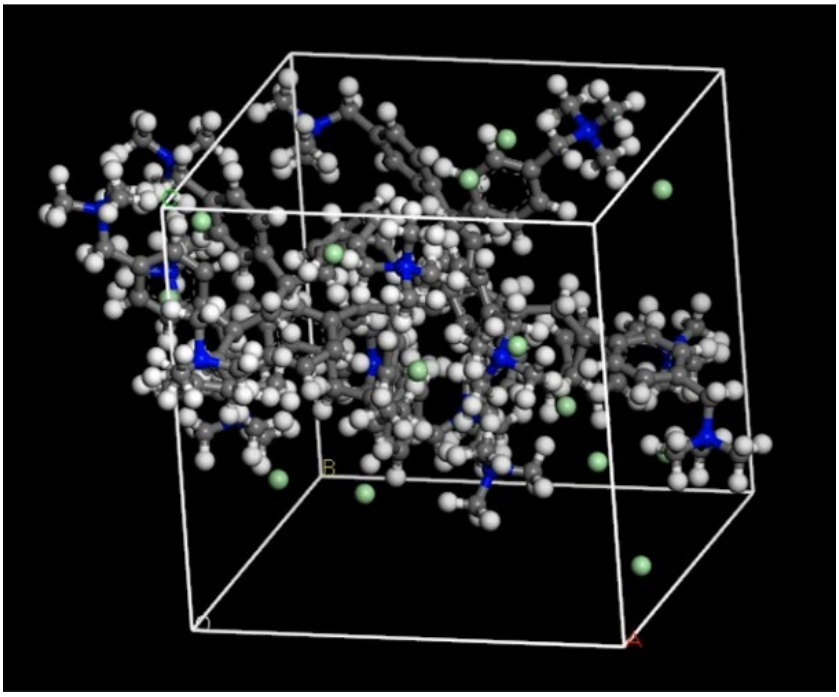

Fig. 3 Membrane slab model with Cl^- ions for DFT simulation (Atom colors: white, H; gray, C; blue, N; and, light green, Cl^-)

The created slab membrane model was structurally optimized using the molecular mechanics method, and DFT simulation was performed to obtain the HOMO/LUMO energy levels of the membrane model. The basis set was used DNP, a functional GGA-RPBE [53] was applied, and the k-point was set to 1x1x1. DNP has been shown to have a sufficiently small basis set superposition error (BSSE)[54], and it can be used in this simulation as well. The convergence conditions for all calculations were set to an energy level of less than 10^{-5} Ha with a maximum force of less than 0.002 Ha/Å and a maximum displacement of less than 0.005 Å. The membrane slab model shown in Fig. 3 was prepared without Cl^- ions, and the

same DFT simulation was performed with the charge set to +14.

3. Results and discussion

3.1. SNP removal and zeta potential measurements in IPA/water solutions

Fig. 4 shows the removal ratio of SNPs in IPA/water solutions with different levels of IPA. The horizontal axis represents the removal time. When the IPA level in the ratio was 0%, the removal rate reached 50% in a short time and increased slowly thereafter. For other IPA ratios, the removal performance could not be improved after more than 1 day of stirring time. Removal was observed, however, following 30 minutes of agitation for IPA levels in the ratio of 10 and 30%. These results indicate that the SNPs were adsorbed onto the membrane surface at 30 min, but subsequently were then desorbed.

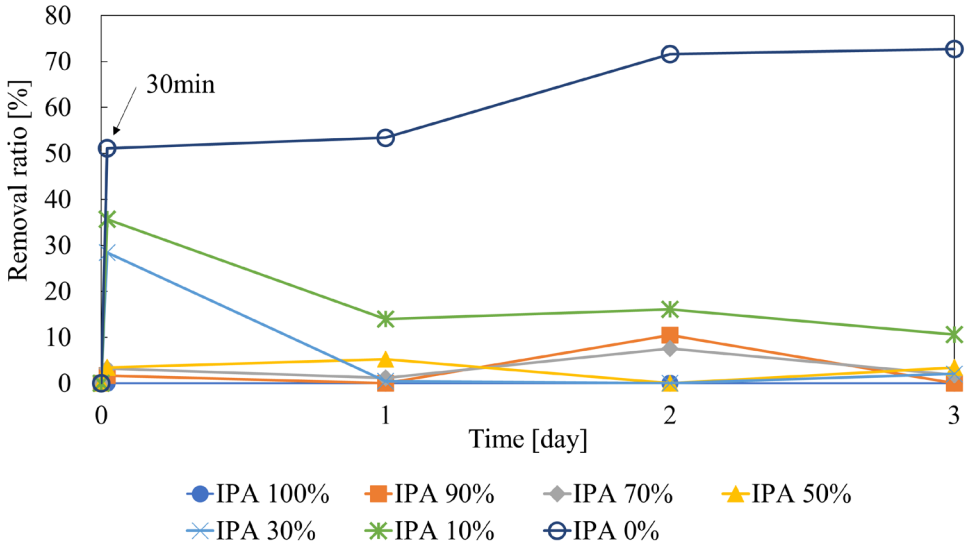

Fig. 4 SNP removal from IPA/water solutions with different concentration ratios

Fig. 5 shows the removal ratio of SNPs when 10 and 100 ppm of NaCl were added after 1 day of stirring under 0% IPA solvent conditions. At this point, however, the SNP removal ratio was decreased because the SNPs that had adsorbed onto the membrane were desorbed by the addition of NaCl.

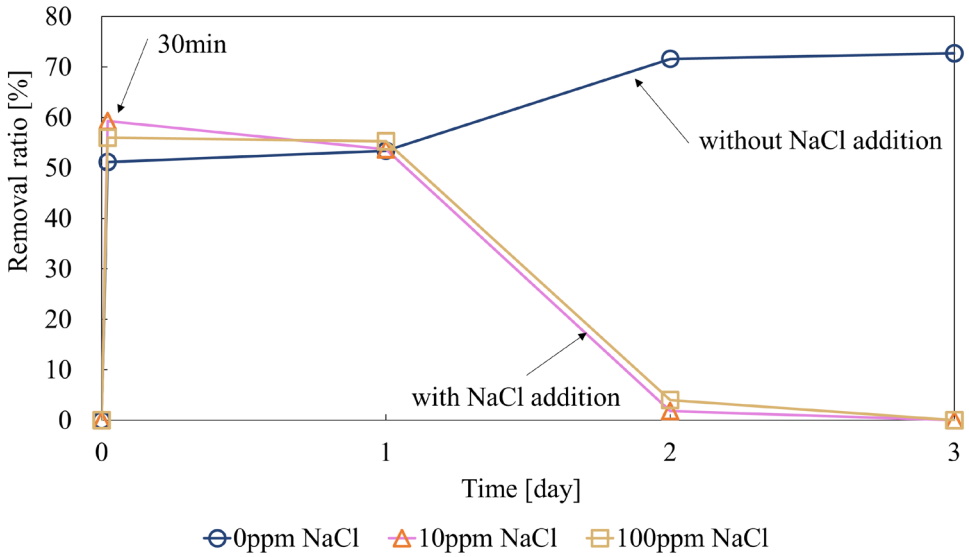

Fig. 5 SNP removal from a solution with a 0% IPA in the ratio with and without NaCl addition after 1 day

The zeta potential results for both the membrane and the SNPs in different concentrations of IPA/water solutions are shown in Fig. 6.

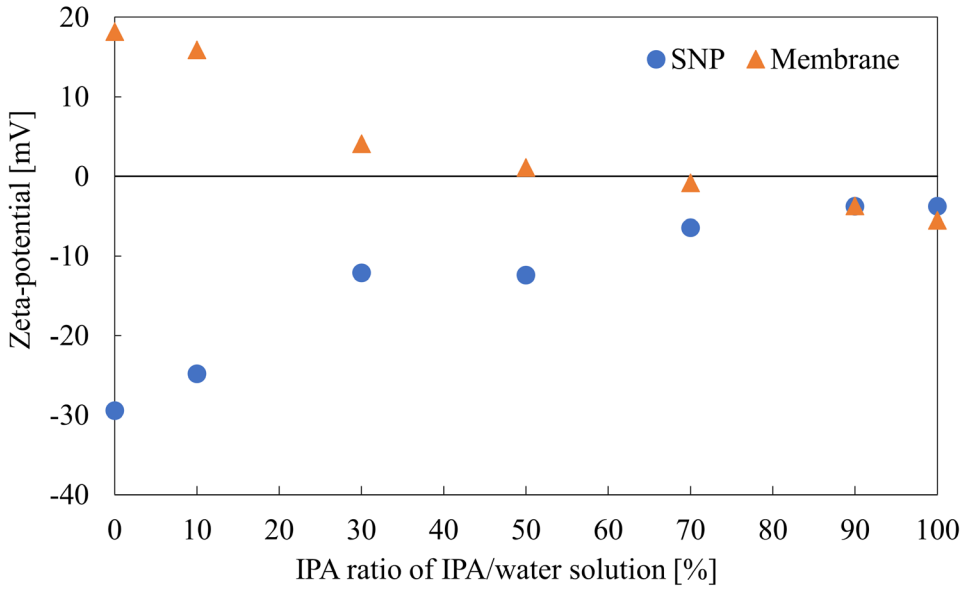

Fig. 6 Zeta potentials of the membrane and SNPs in an IPA/water solution with different concentration ratios

The zeta potential of the SNPs was increased as the IPA level in the ratio increased, and

subsequently approached neutral. The zeta potential remained negative, however, even when the IPA level in the ratio reached 100%. The surface charge of the membrane was almost neutral when the IPA level in the ratio was 50%, and the membrane showed a negative zeta potential when the IPA level exceeded 70%, Removal of the SNPs was prevented when the IPA level in the ratio was higher than 50%. The results of the experiment can be summarized as follows: (1) SNPs were removed via the electrostatic interaction between the membrane and the SNPs; (2) As the IPA level in the ratio increased, the driving force for adsorption was decreased, which decreased the removal performance; (3) When the IPA level in the ratio exceeded 50%, the removal performance was lost due to the lack of a driving force; and, (4) Even when the IPA level in the ratio was 0%, the adsorbed SNPs were desorbed by the addition of NaCl.

3.2. Simulating the molecular dynamics in an IPA/water solution

Fig. 7 shows the results of the c-axis distribution of Cl^- ions for IPA levels in the ratio of 0, 50, and 100% at t = 0, 100, and 250 ps, respectively. The local density distribution was calculated at 4 Å intervals. Snapshots of the MD simulations for each time slot and for each level of IPA in the ratio are shown in Supplementary Fig. 1 (Please refer to the Supplementary Materials link in the online version of this article). Note that the solvent molecules are not drawn in the snapshots in order to facilitate viewing. Fig. 8 shows the transition of total energy in the model with each IPA level in the ratio wherein the calculated model was sufficiently stabilized after 100 ps. Fig. 7 shows that when the IPA level in the ratio was low, the Cl^- ions were diffused from the vicinity of the membrane surface as time passed, and when the IPA level in the ratio was high, the Cl^- ions remained in the vicinity of the membrane and were constrained to the surrounding area.

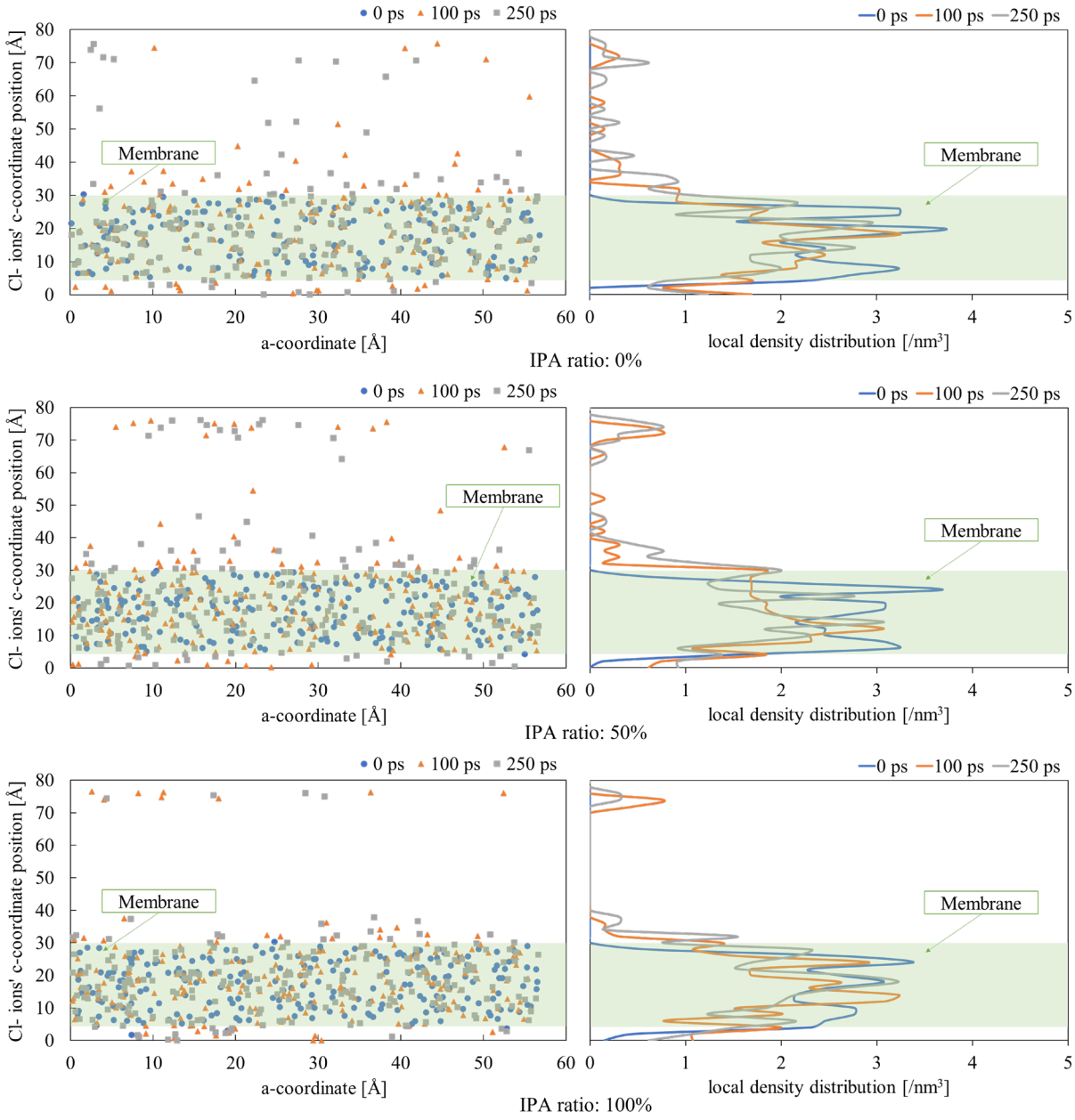

Fig. 7 MD simulation results of Cl^- ions' c-coordinate profiles and local density distribution in IPA/water solutions with levels of IPA in the ratio of 0, 50, and 100%

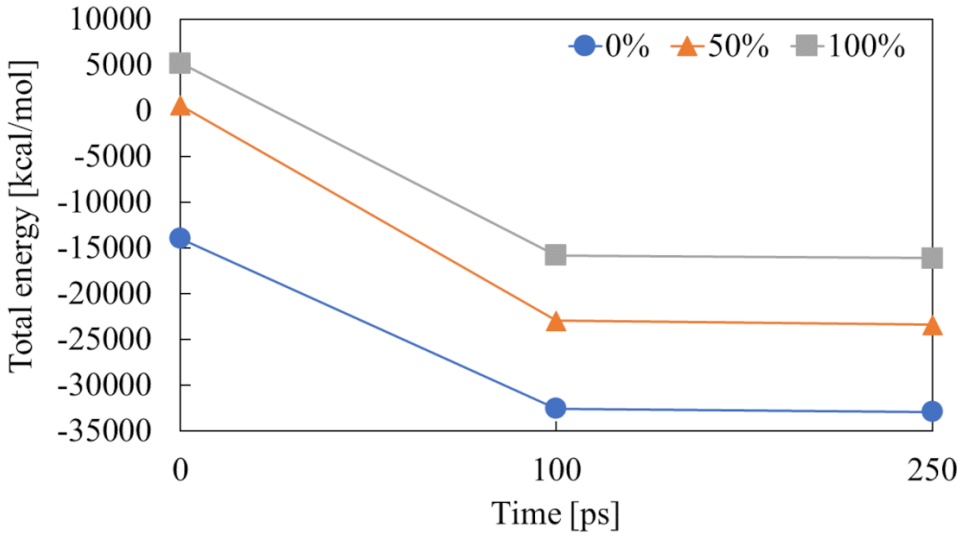

Fig. 8 Total energy transition in IPA/water solutions with levels of IPA in the ratio of 0, 50, and 100%

3.3. Considering the phenomenon whereby the zeta potential of a membrane turns negative

Fig. 7 shows that Cl^- ions were constrained to the vicinity of the membrane when the IPA level in the ratio was high, but were diffused to the bulk when the IPA level in the ratio was low. Therefore, in the DFT simulation model, the membrane model "with Cl^- ions" was regarded as the membrane model in IPA, and the model "without Cl^- ions" was regarded as the membrane model in water. Fig. 9 shows a diagram of the energy level of the membrane slab model (with and without Cl^- ions) obtained from the DFT simulation, along with the HOMO levels of the renormalized solvent molecules, IPA and water [55–57]. The HOMO level of the water/IPA mixture was unknown, but was assumed to be located between the HOMO levels of pure water and IPA.

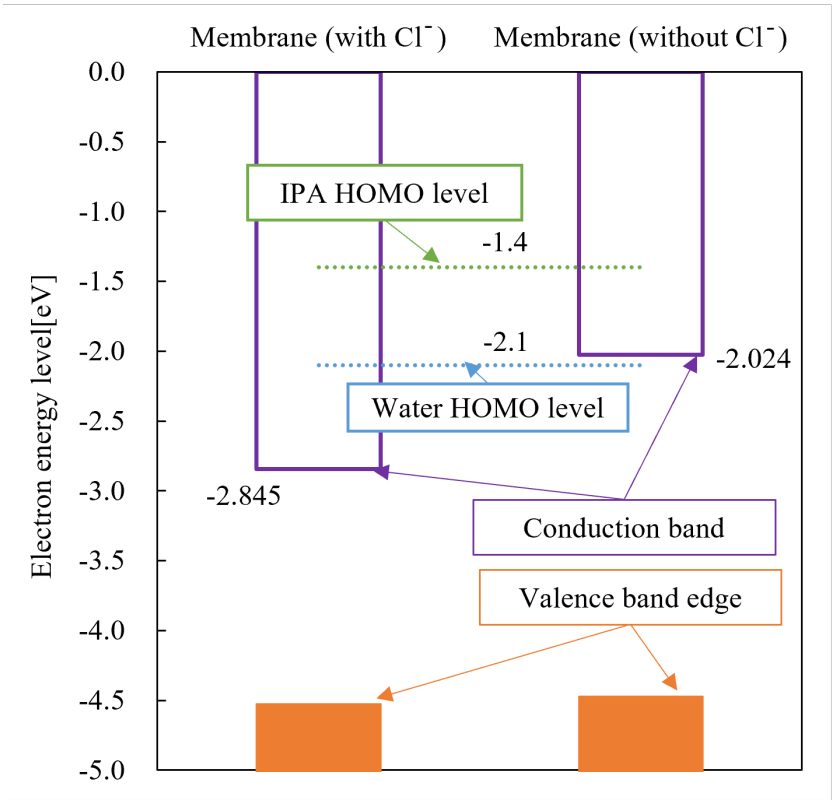

Fig. 9 Diagram of the energy level of a membrane slab model with and without Cl^- ions

Fig. 9 shows that the conduction-band edge of the membrane model with Cl^- ions, i.e., in IPA, was lower than that of the membrane model without Cl^- ions, i.e., in water. The Donor Numbers (DN) of Cl^- ions in methanol and ethanol were -0.98 eV and -1.0624 eV [58], respectively, and the same trend of high electron-donating properties was expected in IPA, where the conduction band edge of the membrane became lower. As a result, the solvent molecules would donate electrons to the membrane model in IPA [57]. Since the HOMO level of IPA is higher than the conduction band edge of the membrane model in IPA, it acts as an electron donor and contributes to the stabilization of the entire system. This suggests that the zeta potential of the membrane immersed in a solvent with a high IPA ratio became negative because it actively received electron donations from the IPA molecules.

On the other hand, the membrane model in water did not receive electron donations from Cl^- ions, and the conduction band edge rose. In addition, the HOMO level of the water molecule was lower than the conduction band edge in the case of the membrane model in water, and, therefore, there were no electron donations from the solvent molecules to the membrane

model. This suggests that the zeta potential of a membrane either in water or in solvents with an IPA level in the ratio of less than 50%, particularly when it is less than 10%, is positive because the membrane receives no electron donations from either the Cl^- ions or the solvent molecules.

From the above discussion and the results shown in Fig. 6, it seems apparent that the HOMO level of the molecules in the mixture solvent and the conduction band edge level of the membrane in the solvent are reversed, and, therefore, the zeta potential of a membrane turns from positive to negative within that range.

As shown in Section 3.1, for IPA levels in the ratio of 10 and 30%, SNPs were removed only after 30 minutes of stirring and were desorbed afterwards. Fig. 4 shows that in the system with 0% IPA in the ratio, SNPs once adsorbed onto the membrane were then desorbed by the additions of 10 and 100 ppm of NaCl. When NaCl was not added, Cl^- ions were present only as counter ions in the membrane. When NaCl was added, however, there was an excess of Cl^- ions in the bulk, which represents the same condition as when Cl^- ions are present in the vicinity of the membrane. Therefore, it seems apparent that the SNPs were desorbed via an exchange with Cl^- ions. These results showed that the desorption after 30 minutes of stirring time in the cases of IPA levels in the ratio of 10 and 30% was caused by a lack of sufficient diffusion by the Cl^- ions from the vicinity of the membrane, which resulted in them being easily exchanged with SNPs. Since AHA was positively charged in water, it was not affected by Na^+ ions and the effect could be ignored. On the other hand, the absolute value of zeta potential of SNP decreases with increasing concentration of NaCl[59], but in this paper, the addition of NaCl has no effect because it is as low as 10 ppm (= 0.171 mM,) 100 ppm (= 1.71 mM). The removal of SNPs is greatly influenced by the surface properties of the ion exchange membrane that vary with the IPA content of the contacted aqueous solution. The useful information on the surface properties could be obtained by even the very short time molecular simulations compared with the actual experimental time. Therefore, we can reasonably assume that the dominant factor of the removal of SNPs could be recognized by the simulation for a limited small scale in a short time. For the removal of SNPs in solvents with high IPA ratios, the understandings of the mechanism obtained in this study would be

applied to a future purification system of IPA/water solutions.

4. Conclusions

In this paper, testing for the removal of SNPs using anion exchange membranes, zeta potential measurements of SNPs and membranes in IPA/water solutions, and MD and DFT simulations were carried out. The zeta potential of the SNPs gradually approached neutral as the IPA level in the ratio increased, but it always remained negative. The zeta potential of the membrane approached neutral, however, when the IPA level in the ratio was about 50%. When the IPA level in the ratio exceeded 70%, the zeta potential turned from positive to negative and the SNPs were not removed. MD and DFT simulations were used to explain these results. MD simulation showed that Cl^- ions were more abundant in the vicinity of the membrane as the level of IPA in the ratio increased. DFT simulations suggested a relationship between the HOMO level of the solvent molecules and the conduction band edge level of the membrane model with and without Cl^- ions, which indicated that the solvent molecules donated electrons to the membrane. In order to remove the negatively charged SNPs in all IPA levels in the ratio, the results of this study showed that the overall design is necessary on the ease of diffusion of counterions near the membrane, the HOMO level of solvent molecules, and the conduction band edge level of the removal membrane.

References

[1] H. Mishima, T. Yasui, T. Mizuniwa, M. Abe, T. Ohmi, Particle-free wafer cleaning and drying technology, IEEE Trans. Semicond. Manuf. 2 (1989) 69–75. https://doi.org/10.1109/66.29672.

[2] T. Ohmi, S. Sudoh, H. Mishima, Static charge removal with IPA solution, IEEE Trans. Semicond. Manuf. 7 (1994) 440–446. https://doi.org/10.1109/66.330281.

[3] S.I. Kudryashov, S.D. Allen, Gas-Phase Transport and Redeposition of Nano- and Micro-Particulates During Laser Cleaning from Solid Substrates, Part. Sci. Technol. 26 (2008) 109–125. https://doi.org/10.1080/02726350701483727.

[4] A. Rastegar, M. Samayoa, M. House, H. Kurtuldu, S.-K. Eah, L. Morse, J.

Harris-Jones, Particle control challenges in process chemicals and ultra-pure water for sub-10nm technology nodes, in: O.R. Wood, E.M. Panning (Eds.), Extrem. Ultrav. Lithogr. V, SPIE, 2014: p. 90480P. https://doi.org/10.1117/12.2048080.

[5] J. Marra, J.A.M. Huethorst, Physical principles of Marangoni drying, Langmuir. 7 (1991) 2748–2755. https://doi.org/10.1021/la00059a057.

[6] X.M. Xu, J. Smeers, G. Vereecke, H. Struyf, Investigation of the Evaporation and Wetting Mechanism of IPA-DIW Mixtures, Solid State Phenom. 195 (2012) 223–226. https://doi.org/10.4028/www.scientific.net/SSP.195.223.

[7] I.D. Mikheev, F.K. Vakhitov, The use of atomic force microscopy to assess the quality of cleaning and tribometric properties of a silicon wafer surface, Comput. Opt. 43 (2019) 507–511. https://doi.org/10.18287/2412-6179-2019-43-3-507-511.

[8] C. Seo, D. Kim, Laser-induced Spray Jet Cleaning Using Isopropyl Alcohol for Nanoparticle Removal from Solid Surfaces, Part. Sci. Technol. 33 (2015) 572–578. https://doi.org/10.1080/02726351.2015.1054974.

[9] Y. Hagimoto, T. Tetsuka, H. Iwamoto, H. Hyakutake, H. Tanaka, Elucidation of an Isopropyl Alcohol (IPA) Adsorption Phenomenon on a Wafer Surface for Achieving an Ultra-Clean and IPA-Saving Drying Process in the Batch Cleaning System, Solid State Phenom. 187 (2012) 79–82. https://doi.org/10.4028/www.scientific.net/SSP.187.79.

[10] Y. Le Tiec, F. Fournel, N. Rochat, J.-P. Barnes, M. Veillerot, C. Morales, H. Moriceau, L. Clavelier, F. Rieutord, C. Morote, M. Vandenbossche, J. Butterbaugh, I. Radu, Drying Impact on Semiconductor Surfaces after Innovative Solvent Exposure, ECS Trans. 25 (2019) 131–138. https://doi.org/10.1149/1.3202645.

[11] T. Koide, S. Kimura, H. Iimori, T. Sugita, K. Sato, S. Kumon, Y. Terui, Y. Okumura, Y. Ogawa, Nano-Structures Stiction Suppression by Molecular Structure Optimized Surface Energy Reduction Agent, ECS Trans. 80 (2017) 53–60. https://doi.org/10.1149/08002.0053ecst.

[12] S.I. Kudryashov, S.D. Allen, S.D. Shukla, Experimental and Theoretical Studies of Laser Cleaning Mechanisms for Submicrometer Particulates on Si Surfaces, Part. Sci.

Technol. 24 (2006) 281–299. https://doi.org/10.1080/02726350600840605.
[13] IRDS, INTERNATIONAL ROADMAP FOR DEVICES AND SYSTEMS 2020 EDITION YIELD ENHANCEMENT, 2020 ed., IEEE, 2020. https://irds.ieee.org/editions/2020/yield-enhancement.
[14] T. Takakura, S. Tsuzuki, Particle removal efficiency evaluation of filters in IPA, in: 2016 Int. Symp. Semicond. Manuf., IEEE, 2016: pp. 1–4. https://doi.org/10.1109/ISSM.2016.7934541.
[15] S. Khezli, M. Zandi, J. Barzin, Fabrication of electrospun nanocomposite polyethersulfone membrane for microfiltration, Polym. Bull. 73 (2016) 2265–2286. https://doi.org/10.1007/s00289-016-1607-5.
[16] C. Duclos-Orsello, W.P. Kelly, D.C. Grant, J. Zahka, V. Thom, Neutral adsorptive capture of particles by membranes: network modeling near the membrane isoelectric point, J. Memb. Sci. 237 (2004) 167–180. https://doi.org/https://doi.org/10.1016/j.memsci.2004.02.030.
[17] Z. Yin, Y. Ma, B. Tanis-Kanbur, J.W. Chew, Fouling behavior of colloidal particles in organic solvent ultrafiltration, J. Memb. Sci. 599 (2020) 117836. https://doi.org/10.1016/j.memsci.2020.117836.
[18] Q.G. Zhang, C. Deng, F. Soyekwo, Q.L. Liu, A.M. Zhu, Sub-10 nm Wide Cellulose Nanofibers for Ultrathin Nanoporous Membranes with High Organic Permeation, Adv. Funct. Mater. 26 (2016) 792–800. https://doi.org/10.1002/adfm.201503858.
[19] Y. Feng, M. Weber, C. Maletzko, T.-S. Chung, Fabrication of organic solvent nanofiltration membranes via facile bioinspired one-step modification, Chem. Eng. Sci. 198 (2019) 74–84. https://doi.org/10.1016/j.ces.2019.01.008.
[20] D. Hua, T.-S. Chung, Polyelectrolyte functionalized lamellar graphene oxide membranes on polypropylene support for organic solvent nanofiltration, Carbon N. Y. 122 (2017) 604–613. https://doi.org/10.1016/j.carbon.2017.07.011.
[21] B. Li, Y. Cui, T.-S. Chung, Hydrophobic Perfluoropolyether-Coated Thin-Film Composite Membranes for Organic Solvent Nanofiltration, ACS Appl. Polym. Mater. 1 (2019) 472–481. https://doi.org/10.1021/acsapm.8b00171.

[22] K.S. Goh, J.Y. Chong, Y. Chen, W. Fang, T.-H. Bae, R. Wang, Thin-film composite hollow fibre membrane for low pressure organic solvent nanofiltration, J. Memb. Sci. 597 (2020) 117760. https://doi.org/10.1016/j.memsci.2019.117760.

[23] L.-F. Fang, M.-Y. Zhou, L. Cheng, B.-K. Zhu, H. Matsuyama, S. Zhao, Positively charged nanofiltration membrane based on cross-linked polyvinyl chloride copolymer, J. Memb. Sci. 572 (2019) 28–37. https://doi.org/https://doi.org/10.1016/j.memsci.2018.10.054.

[24] K. Yamamoto, T. Ogawa, M. Matsuda, A. Iino, T. Yakushiji, T. Miyasaka, K. Sakai, Membrane potential and charge density of hollow-fiber dialysis membranes, J. Memb. Sci. 355 (2010) 182–185. https://doi.org/https://doi.org/10.1016/j.memsci.2010.03.023.

[25] J. Schaep, C. Vandecasteele, Evaluating the charge of nanofiltration membranes, J. Memb. Sci. 188 (2001) 129–136. https://doi.org/https://doi.org/10.1016/S0376-7388(01)00368-4.

[26] M.D. Afonso, Surface charge on loose nanofiltration membranes, Desalination. 191 (2006) 262–272. https://doi.org/https://doi.org/10.1016/j.desal.2005.04.127.

[27] M. Tarek, M.L. Klein, Molecular Dynamics Study of Two-Component Systems: The Shape and Surface Structure of Water/Ethanol Droplets, J. Phys. Chem. A. 101 (1997) 8639–8642. https://doi.org/10.1021/jp972278s.

[28] M. Lundgren, N.L. Allan, T. Cosgrove, N. George, Wetting of Water and Water/Ethanol Droplets on a Non-Polar Surface: A Molecular Dynamics Study, Langmuir. 18 (2002) 10462–10466. https://doi.org/10.1021/la026191w.

[29] T.-M. Chang, L.X. Dang, Liquid−Vapor Interface of Methanol−Water Mixtures: A Molecular Dynamics Study, J. Phys. Chem. B. 109 (2005) 5759–5765. https://doi.org/10.1021/jp045649v.

[30] D. Surblys, Y. Yamaguchi, K. Kuroda, M. Kagawa, T. Nakajima, H. Fujimura, Molecular dynamics analysis on wetting and interfacial properties of water-alcohol mixture droplets on a solid surface, J. Chem. Phys. 140 (2014) 34505. https://doi.org/10.1063/1.4861039.

[31] L.A. Melnik, D.A. Krysenko, Ultrapure Water: Properties, Production, and Use, J. Water Chem. Technol. 41 (2019) 143–150. https://doi.org/10.3103/S1063455X19030020.
[32] J. Ruth, R. Berndt, Quality Control for Ultrafiltration of Ultrapure Water Production for High End Semiconductor Manufacturing, in: 2016 27TH Annu. SEMI Adv. Semicond. Manuf. Conf., 2016: pp. 16–22.
[33] T. Hori, M. Hashino, A. Omori, T. Matsuda, K. Takasa, K. Watanabe, Synthesis of novel microfilters with ion-exchange capacity and its application to ultrapure water production systems, J. Memb. Sci. 132 (1997) 203–211. https://doi.org/https://doi.org/10.1016/S0376-7388(97)00076-8.
[34] Q. Chan, M. Entezarian, J. Zhou, R. Osterloh, Q. Huang, M. Ellefson, B. Mader, Y. Liu, M. Swierczek, Gold nanoparticle mixture retention test with single particle detection: A fast and sensitive probe for functional pore sizes of ultrafiltration membranes, J. Memb. Sci. 599 (2020) 117822. https://doi.org/10.1016/j.memsci.2020.117822.
[35] Z.-W. Dai, J. Ling, X.-J. Huang, L.-S. Wan, Z.-K. Xu, Molecular Simulation on the Interactions of Water with Polypropylene Surfaces, J. Phys. Chem. C. 115 (2011) 10702–10708. https://doi.org/10.1021/jp201040g.
[36] Z.-W. Dai, L.-S. Wan, X.-J. Huang, J. Ling, Z.-K. Xu, Selective Adsorption of Isopropyl Alcohol Aqueous Solution on Polypropylene Surfaces: A Molecular Dynamics Simulation, J. Phys. Chem. C. 115 (2011) 22415–22421. https://doi.org/10.1021/jp206733b.
[37] V.I. Kuchuk, I.Y. Shirokova, E. V Golikova, Physicochemical properties of water-alcohol mixtures of a homological series of lower aliphatic alcohols, Glas. Phys. Chem. 38 (2012) 460–465. https://doi.org/10.1134/S1087659612050057.
[38] F.-M. Pang, C.-E. Seng, T.-T. Teng, M.H. Ibrahim, Densities and viscosities of aqueous solutions of 1-propanol and 2-propanol at temperatures from 293.15 K to 333.15 K, J. Mol. Liq. 136 (2007) 71–78. https://doi.org/10.1016/j.molliq.2007.01.003.
[39] J.-G. Park, S.-H. Lee, J.-S. Ryu, Y.-K. Hong, T.-G. Kim, A.A. Busnaina, Interfacial

and Electrokinetic Characterization of IPA Solutions Related to Semiconductor Wafer Drying and Cleaning, J. Electrochem. Soc. 153 (2006) G811. https://doi.org/10.1149/1.2214532.

[40] H. Sun, COMPASS: An ab Initio Force-Field Optimized for Condensed-Phase ApplicationsOverview with Details on Alkane and Benzene Compounds, J. Phys. Chem. B. 102 (1998) 7338–7364. https://doi.org/10.1021/jp980939v.

[41] H. Sun, Z. Jin, C. Yang, R.L.C. Akkermans, S.H. Robertson, N.A. Spenley, S. Miller, S.M. Todd, COMPASS II: extended coverage for polymer and drug-like molecule databases, J. Mol. Model. 22 (2016) 1–10. https://doi.org/10.1007/s00894-016-2909-0.

[42] H. Moradi, H. Azizpour, H. Bahmanyar, M. Mohammadi, M. Akbari, Prediction of methane diffusion coefficient in water using molecular dynamics simulation, Heliyon. 6 (2020) e05385. https://doi.org/10.1016/j.heliyon.2020.e05385.

[43] J.Y. Wu, Q.L. Liu, Y. Xiong, A.M. Zhu, Y. Chen, Molecular simulation of water/alcohol mixtures' adsorption and diffusion in zeolite 4a membranes, J. Phys. Chem. B. 113 (2009) 4267–4274. https://doi.org/10.1021/jp805923k.

[44] D. Rigby, Fluid density predictions using the COMPASS force field, Fluid Phase Equilib. 217 (2004) 77–87. https://doi.org/10.1016/j.fluid.2003.08.019.

[45] B. Thomson, A. Rudin, G. Lajoie, Dispersion copolymerization of styrene and divinylbenzene: Synthesis of monodisperse, uniformly crosslinked particles, J. Polym. Sci. Part A Polym. Chem. 33 (1995) 345–357. https://doi.org/https://doi.org/10.1002/pola.1995.080330301.

[46] W. Yang, W. Ming, J. Hu, X. Lu, S. Fu, Morphological investigations of crosslinked polystyrene microspheres by seeded polymerization, Colloid Polym. Sci. 276 (1998) 655–661. https://doi.org/10.1007/s003960050294.

[47] H.J.C. Berendsen, J.P.M. Postma, W.F. van Gunsteren, A. DiNola, J.R. Haak, Molecular dynamics with coupling to an external bath, J. Chem. Phys. 81 (1984) 3684–3690. https://doi.org/10.1063/1.448118.

[48] S. Nosé, A molecular dynamics method for simulations in the canonical ensemble, Mol. Phys. 52 (1984) 255–268. https://doi.org/10.1080/00268978400101201.

[49] S. Nosé, A unified formulation of the constant temperature molecular dynamics methods, J. Chem. Phys. 81 (1984) 511–519. https://doi.org/10.1063/1.447334.
[50] N. Shuichi, Constant Temperature Molecular Dynamics Methods, Prog. Theor. Phys. Suppl. 103 (1991) 1–46. https://doi.org/10.1143/PTPS.103.1.
[51] V. Černý, Thermodynamical approach to the traveling salesman problem: An efficient simulation algorithm, J. Optim. Theory Appl. 45 (1985) 41–51. https://doi.org/10.1007/BF00940812.
[52] S. Kirkpatrick, C.D. Gelatt, M.P. Vecchi, Optimization by Simulated Annealing, Science (80-.). 220 (1983) 671–680. https://doi.org/10.1126/science.220.4598.671.
[53] B. Hammer, L.B. Hansen, J.K. Norskov, Improved adsorption energetics within density-functional theory using revised Perdew-Burke-Ernzerhof functionals, Phys. Rev. B. 59 (1999) 7413–7421. https://doi.org/10.1103/PhysRevB.59.7413.
[54] Y. Inada, H. Orita, Efficiency of numerical basis sets for predicting the binding energies of hydrogen bonded complexes: Evidence of small basis set superposition error compared to Gaussian basis sets, J. Comput. Chem. 29 (2008) 225–232. https://doi.org/https://doi.org/10.1002/jcc.20782.
[55] V. Gutmann, The Donor-Acceptor Approach to Molecular Interactions, Springer US, Boston, MA, 1978. https://doi.org/10.1007/978-1-4615-8825-2.
[56] V. Gutmann, Solvent effects on the reactivities of organometallic compounds, Coord. Chem. Rev. 18 (1976) 225–255. https://doi.org/https://doi.org/10.1016/S0010-8545(00)82045-7.
[57] V. Pande, V. Viswanathan, Descriptors for Electrolyte-Renormalized Oxidative Stability of Solvents in Lithium-Ion Batteries, J. Phys. Chem. Lett. 10 (2019) 7031–7036. https://doi.org/10.1021/acs.jpclett.9b02717.
[58] W. Linert, R.F. Jameson, A. Taha, Donor numbers of anions in solution: the use of solvatochromic Lewis acid–base indicators, J. Chem. Soc. Dalt. Trans. (1993) 3181–3186. https://doi.org/10.1039/DT9930003181.
[59] M.A. Brown, A. Goel, Z. Abbas, Effect of Electrolyte Concentration on the Stern Layer Thickness at a Charged Interface, Angew. Chemie - Int. Ed. 55 (2016) 3790–

3794. https://doi.org/10.1002/anie.201512025.